Size dependent bending analysis of two directional functionally graded microbeams via a quasi-3D theory and finite element method

Armağan Karamanlı[1,‡] , Thuc P. Vo[2]

[1] Department of Mechatronics, Faculty of Engineering and Architecture, Istanbul Gelişim University, 34215,Istanbul, Turkey.

[2] Department of Mechanical and Construction Engineering, Northumbria University, Ellison Place, Newcastle upon Tyne NE1 8ST, UK

‡ Corresponding Author; Armağan Karamanlı, Istanbul Gelişim University, 34215, Istanbul, Turkey, Tel: +90 212 422 7020, armagan_k@yahoo.com

Abstract

This paper presents the flexural behaviour of two directional functionally graded (2D-FG) microbeams subjected to uniformly distributed load with various boundary conditions. A four-unknown shear and normal deformation theory or quasi-3D one is employed based on the modified couple stress theory, Ritz method and finite element formulation. The material properties are assumed to vary through the thickness and longitudinal axis and follow the power-law distribution. Firstly, the static deformations of conventional FG microbeams are investigated to verify the developed finite element code. For the convergence studies, a simply supported FG microbeam is considered by employing various number of elements in the problem domain, aspect ratios, material length scale parameters and gradient indexes. The verification of the developed code is established and then extensive studies are performed for various boundary conditions. Secondly, since there is no reported data regarding to the analysis of 2D-FG microbeams, verification studies are performed for 2D-FG beams with different aspect ratios and gradient indexes. The effects of the normal and shear deformations as well as and material length scale parameters on the flexural behaviour of the 2D-FG microbeams are investigated. Finally, some new results for deflections of conventional FG and 2D-FG microbeams for various boundary conditions are introduced for the first time and can be used as reference for future studies.

Keywords: 2D Functionally Graded Microbeam, Finite Element Method, Quasi-3D Theory, Modified Couple Stress Theory.

1. Introduction

In most of the research and development activities, one of the biggest problems of engineers is the selection of the proper material which can satisfy all the technical and economical requirements. A group of Japanese scientists introduced a novel material called as Functionally Graded Material (FGM) in 1984 for the manufacturing of a thermal barrier to withstand very high surface temperature and work in severe operating conditions [1]. FGMs can be classified as advanced materials whose material properties vary continuously in the desired directions. The advantages of using these materials over the conventional composites are avoiding the stress concentration, cracking and interface problems. FGMs have been using in many engineering areas such as military, aerospace, nuclear energy, biomedical, and electrical engineering for nano/micro devices. Researchers have been developed different theories and methods of analysis to predict and understand precisely their behaviours especially in very small scales. Due to its computational efficiency, the non-classical continuum approach has been used widely to analyse the size dependent behaviour of small scale structures. Yang et al. [2] proposed the modified couple stress theory (MCST) by modifying the classical couple stress theory [3-6] and more importantly only one material length scale parameter is required. This theory has been used by the many researchers to analyse the bending, vibration and buckling behaviours of isotropic, laminated composite and conventional FG beams based on various theories such as Euler-Bernoulli beam theory, first-order beam theory (FBT), higher-order beam theory (HBT) as well as shear and normal beam theory or quasi-3D one [7-43]. More details about size-dependent models including the MCST, non-local elasticity [44-51] and strain gradient [52-54] can be found in recent works of Romano et al. [55] and Thai et al. [56]. The conventional FGMs may not be effective for aerospace craft and shuttles in the severe operation conditions since the distribution of temperature and stress in these structures varies in two or three directions [57]. Therefore, 2D-FG beams whose material properties vary in two directions are proposed. Goupee and Vel [58] optimise the first three natural frequencies of 2D-FG beams using the element free Galerkin method. Elasticity solutions for static bending and thermal deformation of 2D-FG beams are derived by Lu et al. [59] using the combination of state space approach and differential quadrature method. Zhao et al. [60] study bending and vibration analysis of 2D-FG beams by using a symplectic elasticity solution. Simsek [61-62] investigates free, and forced vibration as well as buckling of Timoshenko 2D-FG beams, whose material properties follow the power-law distribution. Karamanli [63] presents the static behaviour of 2D-FG beams by using various theories. The coupled thermo-mechanical response of 2D-FG beams is studied by Nazargah [64] via finite element method (FEM). Pydah and Batra

[65] derive an analytical solution for deflections of the 2D-FG circular beams. Karamanli [66] studies the flexure behaviour of the 2D-FG sandwich beams by using a quasi-3D theory and a meshless method. Some recents contributions dealing with the Saint-Venant beams can also be found in [67-69]. Regarding to the studies based on the non-local classical methods, the bending, vibration and buckling problems of 2D-FG nanobeams are analysed by Nejad et al. [70-72]. Shafiei and Kazemi [73] present the buckling behaviour of 2D-FG porous tapered Euler Bernoulli micro/nano beams. By using the FBT, the vibration of imperfect 2D-FG micro/nano beams is investigated by Shafiei et al. [74]. Recently, the vibration behaviour of 2D-FG microbeams with arbitrary boundary conditions is presented by Trinh et al. [75] using the HBT and quasi-3D theory based on the MCST. According to the best of the authors' knowledge, there is no study dealing with the flexural behaviour of the 2D-FG microbeams with various boundary conditions using a quasi-3D theory. This complicated problem is solved here for the first time by FEM, which is also the main novelty of current paper. Numerical examples are presented for various aspect ratios, gradient indexes and material length scale parameters to investigate the flexural behaviours of the conventional FG and 2D-FG microbeams with arbitrary boundary conditions.

2. Theory and Formulation

2.1 Two Directional Functionally Graded (2D-FG) Microbeams

A 2D-FG microbeam with rectangular section (bxh), length (L), and its bending plane as x-z is illustrated in Fig. 1. It should be noted that only microbeams under uniaxial flexure are considered in this study. The material properties vary both longitudinal and thickness directions. The rule of mixture is used to estimate the Young's moduli E and Poisson's ratio ν:

Figure 1 Right Here

$$E(x,z) = E_1 V_1(x,z) + E_2 V_2(x,z) \quad (1a)$$

$$\nu(x,z) = \nu_1 V_1(x,z) + E_2 \nu_2(x,z) \quad (1b)$$

Where E_1 and E_2 are Young's moduli, ν_1 and ν_2 are Poisson's ratio, V_1 and V_2 are volume fractions of two constituents. According to the power-law rule, the relation of V_1 and V_2 can be given

$$V_1(x,z) + V_2(x,z) = 1 \tag{2}$$

where

$$V_1(x,z) = \left(1 - \frac{x}{2L}\right)^{p_x} \left(\frac{1}{2} + \frac{z}{h}\right)^{p_z} \tag{3}$$

here p_x and p_z are the gradient or power-law indexes in *x*- and *z*-direction.

By using Eqs. (1)-(3), Young's moduli E and Poisson's ratio ν can be found by as follows:

$$E(x,z) = (E_1 - E_2)\left(1 - \frac{x}{2L}\right)^{p_x} \left(\frac{1}{2} + \frac{z}{h}\right)^{p_z} + E_2 \tag{4a}$$

$$\nu(x,z) = (\nu_1 - \nu_2)\left(1 - \frac{x}{2L}\right)^{p_x} \left(\frac{1}{2} + \frac{z}{h}\right)^{p_z} + \nu_2 \tag{4b}$$

2.2 Modified Couple Stress Theory (MCST)

According to the MCST, the strain energy ($\mathcal{U}$) of a deformed isotropic linear elastic body occupying a volume V can be written as follows [1]:

$$\mathcal{U} = \frac{1}{2}\int_V \left(\sigma_{ij}\varepsilon_{ij} + m_{ij}\chi_{ij}\right) dV, \quad i,j = 1,2,3 \tag{5}$$

where σ_{ij} is the stress tensor, ε_{ij} is the strain tensor, m_{ij} is the deviatoric part of the symmetric couple stress tensor and χ_{ij} is the symmetric curvature tensor. The components of χ_{ij} are given by:

$$\chi_{ij} = \frac{1}{2}\left(\frac{\partial \theta_i}{\partial x_j} + \frac{\partial \theta_j}{\partial x_i}\right) \qquad i,j = 1,2,3 \tag{6}$$

where θ_i is the components of the rotation vector related to the displacement field (u_1, u_2, u_3) as:

$$\theta_i = \frac{1}{2} e_{ijk} u_{k,j} \qquad i,j,k = 1,2,3 \tag{7c}$$

where e_{ijk} is the permutation symbol.

2.3 Kinematics and Constitutive Relations

The effects of shear and normal deformations are included in the displacement field below [43, 60, 63, 69]:

$$\begin{aligned} u_1(x,z,t) = U(x,z,t) &= u(x,t) - z\frac{\partial w_b(x,t)}{\partial x} - \frac{4z^3}{3h^2}\frac{\partial w_s(x,t)}{\partial x} \\ &= u(x,t) - z w_b'(x,t) - f(z) w_s'(x,t) \end{aligned} \tag{8a}$$

$$u_3(x,z,t) = W(x,z,t) = w_b(x,t) + w_s(x,t) + \left(1 - \frac{4z^2}{h^2}\right) w_z(x,t)$$

$$= w_b(x,t) + w_s(x,t) + g(z)w_z(x,t) \tag{8b}$$

where u, w_b, w_s and w_z are the mid-plane displacements of the axial, bending, shear and thickness stretching components. The prime notation is used to represent the derivative of the displacements with respect to *x*.

The nonzero strains can be written as:

$$\varepsilon_x = \frac{\partial U}{\partial x} = u' - zw_b'' - f(z)w_s'' \tag{9a}$$

$$\varepsilon_z = \frac{\partial W}{\partial z} = g'(z)w_z \tag{9b}$$

$$\gamma_{xz} = \frac{\partial W}{\partial x} + \frac{\partial U}{\partial z} = g(z)(w_s' + w_z') \tag{9c}$$

The rotation vector can be obtained by using Eqs. (7) and (8):

$$\theta_y = \tfrac{1}{2}\left(\tfrac{\partial U}{\partial z} - \tfrac{\partial W}{\partial x}\right) = -w_b' - \tfrac{1}{2}(1+f')w_s' - \tfrac{1}{2}gw_z' \tag{10a}$$

$$\theta_x = 0, \theta_z = 0 \tag{10b}$$

By using Eq. (10), the components of the symmetric curvature tensor can be written as:

$$\chi_{xy} = \frac{1}{2}\left(\frac{\partial \theta_x}{\partial y} + \frac{\partial \theta_y}{\partial x}\right) = \frac{1}{2}\left[-w_b'' - \frac{1}{2}(1+f')w_s'' - \frac{1}{2}gw_z''\right] \tag{11a}$$

$$\chi_{yz} = \frac{1}{2}\left(\frac{\partial \theta_z}{\partial y} + \frac{\partial \theta_y}{\partial z}\right) = \frac{1}{4}(-f''w_s' - g'w_z') \tag{11b}$$

$$\chi_{xx} = \chi_{yy} = \chi_{zz} = \chi_{xz} = 0 \tag{11c}$$

The following linear elastic constitutive relations for 2D-FG microbeams can be written:

$$\begin{Bmatrix} \sigma_x \\ \sigma_z \\ \sigma_{xz} \end{Bmatrix} = \frac{E(x,z)}{1-\nu^2(x,z)} \begin{bmatrix} 1 & \nu(x,z) & 0 \\ \nu(x,z) & 1 & 0 \\ 0 & 0 & \frac{1-\nu(x,z)}{2} \end{bmatrix} \begin{Bmatrix} \varepsilon_x \\ \varepsilon_z \\ \gamma_{xz} \end{Bmatrix} \tag{12a}$$

$$\begin{Bmatrix} m_{xy} \\ m_{yz} \end{Bmatrix} = \frac{E(x,z)\ell^2}{1+\nu(x,z)} \begin{Bmatrix} \chi_{xy} \\ \chi_{yz} \end{Bmatrix} \tag{12b}$$

where ℓ is the material length scale parameter [1], which can be determined from microscale experiments (i.e., microtorsion or microbending tests) [43, 54].

2.4 Variational Formulation

The strain energy of a 2D-FG microbeam can be written based on the displacement field given above as:

$$\mathcal{U} = \frac{1}{2}\int_V (\sigma_x\varepsilon_x + \sigma_z\varepsilon_z + \sigma_{xz}\gamma_{xz} + 2m_{xy}\chi_{xy} + 2m_{yz}\chi_{yz})dV \tag{13}$$

The following form of the strain energy can be written by substituting Eq. (12) into Eq. (13):

$$\mathcal{U} = \frac{1}{2}\int_V \left[\frac{E}{1-\nu^2}\left(\varepsilon_x\varepsilon_x + 2\nu\varepsilon_x\varepsilon_z + \varepsilon_z\varepsilon_z + \frac{1-\nu}{2}\gamma_{xz}\gamma_{xz}\right) + \frac{E\ell^2}{1+\nu}\left(2\chi_{xy}\chi_{xy} + 2\chi_{yz}\chi_{yz}\right)\right]dV \tag{14}$$

where

$$\varepsilon_x\varepsilon_x = \left(\frac{du}{dx}\right)^2 + z^2\left(\frac{d^2w_b}{dx^2}\right)^2 + f^2\left(\frac{d^2w_s}{dx^2}\right)^2 - 2z\left(\frac{du}{dx}\right)\left(\frac{d^2w_b}{dx^2}\right) - 2f\left(\frac{du}{dx}\right)\left(\frac{d^2w_s}{dx^2}\right) + 2fz\left(\frac{d^2w_b}{dx^2}\right)\left(\frac{d^2w_s}{dx^2}\right) \tag{15a}$$

$$\varepsilon_x\varepsilon_z = \left(\frac{dg}{dz}\right)\left(\frac{du}{dx}\right)w_z - \left(\frac{dg}{dz}\right)z\left(\frac{d^2w_b}{dx^2}\right)w_z - \left(\frac{dg}{dz}\right)f\left(\frac{d^2w_s}{dx^2}\right)w_z \tag{15b}$$

$$\varepsilon_z\varepsilon_z = \left(\frac{dg}{dz}\right)^2 {w_z}^2 \tag{15c}$$

$$\gamma_{xz}\gamma_{xz} = g^2\left(\frac{dw_s}{dx}\right)^2 + g^2\left(\frac{dw_z}{dx}\right)^2 + 2g^2\left(\frac{dw_s}{dx}\right)\left(\frac{dw_z}{dx}\right) \tag{15d}$$

$$\chi_{xy}\chi_{xy} = \frac{1}{4}\left[\left(\frac{d^2w_b}{dx^2}\right)^2 + \frac{1}{4}\left(1+\frac{df}{dz}\right)^2\left(\frac{d^2w_s}{dx^2}\right)^2 + \frac{1}{4}g^2\left(\frac{d^2w_z}{dx^2}\right)^2 + \left(1+\frac{df}{dz}\right)\left(\frac{d^2w_b}{dx^2}\right)\left(\frac{d^2w_s}{dx^2}\right) + g\left(\frac{d^2w_b}{dx^2}\right)\left(\frac{d^2w_z}{dx^2}\right) + \frac{1}{2}\left(1+\frac{df}{dz}\right)g\left(\frac{d^2w_s}{dx^2}\right)\left(\frac{d^2w_z}{dx^2}\right)\right] \tag{15e}$$

$$\chi_{yz}\chi_{yz} = \frac{1}{16}\left[\left(\frac{d^2f}{dz^2}\right)^2\left(\frac{dw_s}{dx}\right)^2 + \left(\frac{dg}{dz}\right)^2\left(\frac{dw_z}{dx}\right)^2 + 2\left(\frac{d^2f}{dz^2}\right)\left(\frac{dg}{dz}\right)\left(\frac{dw_s}{dx}\right)\left(\frac{dw_z}{dx}\right)\right] \tag{15f}$$

It is convenient to introduce the stiffness coefficients as follows:

$$(A, B, B_s, D, D_s, H, Z) = b\int_{-h/2}^{+h/2}\frac{(E_1 - E_2)}{1-\nu^2}\left(\frac{1}{2}+\frac{z}{h}\right)^{p_z}(1, z, f, z^2, fz, f^2, g'^2)dz \tag{16a}$$

$$(A_1, B_1, B_{s1}, D_1, D_{s1}, H_1, Z_1) = b\int_{-h/2}^{+h/2}\frac{E_2}{1-\nu^2}(1, z, f, z^2, fz, f^2, g'^2)dz \tag{16b}$$

$$A_s = b\int_{-h/2}^{+h/2}\frac{(E_1 - E_2)}{2(1+\nu)}\left(\frac{1}{2}+\frac{z}{h}\right)^{p_z}g^2dz \tag{16c}$$

$$A_{s1} = b\int_{-h/2}^{+h/2}\frac{E_2}{2(1+\nu)}g^2dz \tag{16d}$$

$$(X, Y, Y_s) = b\int_{-h/2}^{+h/2} \frac{(E_1 - E_2)\nu}{1-\nu^2}\left(\frac{1}{2}+\frac{z}{h}\right)^{p_z} g'(1, z, f)dz \tag{16e}$$

$$(X_1, Y_1, Y_{s1}) = b\int_{-h/2}^{+h/2} \frac{E_2\nu}{1-\nu^2} g'(1, z, f)dz \tag{16f}$$

$$(A_n, B_n, C_n, D_n, F_n, H_n, X_n, Y_n, Z_n)$$
$$= b\int_{-h/2}^{+h/2} \frac{(E_1 - E_2)\ell^2}{1+\nu}\left(\frac{1}{2}+\frac{z}{h}\right)^{p_z} [1, (1+f'), (1+f')^2, g, g^2, (1+f')g, (f'')^2, (g')^2, f''g']dz \tag{16g}$$

$$(A_{n1}, B_{n1}, C_{n1}, D_{n1}, F_{n1}, H_{n1}, X_{n1}, Y_{n1}, Z_{n1})$$
$$= b\int_{-h/2}^{+h/2} \frac{E_2\ell^2}{1+\nu} [1, (1+f'), (1+f')^2, g, g^2, (1+f')g, (f'')^2, (g')^2, f''g']dz \tag{16h}$$

The potential energy by the uniformly distributed load q(x) is given by

$$\mathcal{V} = \int_{-\frac{L}{2}}^{\frac{L}{2}} q[w_b + w_s + g(z)w_z]dx \tag{17}$$

Using Eqs. (14) to (17), the total potential energy (Π) can be written in the form of:

$$\Pi = \mathcal{U} + \mathcal{V}$$

$$\Pi = \frac{1}{2}\int_0^L \left[\left\{A\left(1-\frac{x}{2L}\right)^{p_x} + A_1\right\}\left(\frac{du}{dx}\right)^2 + \left\{D\left(1-\frac{x}{2L}\right)^{p_x} + D_1\right\}\left(\frac{d^2w_b}{dx^2}\right)^2\right.$$
$$+\left\{H\left(1-\frac{x}{2L}\right)^{p_x} + H_1\right\}\left(\frac{d^2w_s}{dx^2}\right)^2 + 2\left\{D_s\left(1-\frac{x}{2L}\right)^{p_x} + D_{s1}\right\}\left(\frac{d^2w_b}{dx^2}\right)\left(\frac{d^2w_s}{dx^2}\right)$$
$$-2\left\{B\left(1-\frac{x}{2L}\right)^{p_x} + B_1\right\}\left(\frac{du}{dx}\right)\left(\frac{d^2w_b}{dx^2}\right) - 2\left\{B_s\left(1-\frac{x}{2L}\right)^{p_x} + B_{s1}\right\}\left(\frac{du}{dx}\right)\left(\frac{d^2w_s}{dx^2}\right)$$
$$+2\left\{X\left(1-\frac{x}{2L}\right)^{p_x} + X_1\right\}\left(\frac{du}{dx}\right)w_z - 2\left\{Y\left(1-\frac{x}{2L}\right)^{p_x} + Y_1\right\}\left(\frac{d^2w_b}{dx^2}\right)w_z$$
$$-2\left\{Y_s\left(1-\frac{x}{2L}\right)^{p_x} + Y_{s1}\right\}\left(\frac{d^2w_s}{dx^2}\right)w_z + \left\{Z\left(1-\frac{x}{2L}\right)^{p_x} + Z_1\right\}{w_z}^2$$
$$+\left\{A_s\left(1-\frac{x}{2L}\right)^{p_x} + A_{s1}\right\}\left\{\left(\frac{dw_s}{dx}\right)^2 + \left(\frac{dw_z}{dx}\right)^2 + 2\left(\frac{dw_s}{dx}\right)\left(\frac{dw_z}{dx}\right)\right\}$$
$$+\frac{1}{2}\left\{A_n\left(1-\frac{x}{2L}\right)^{p_x} + A_{n1}\right\}\left(\frac{d^2w_b}{dx^2}\right)^2 + \frac{1}{8}\left\{C_n\left(1-\frac{x}{2L}\right)^{p_x} + C_{n1}\right\}\left(\frac{d^2w_s}{dx^2}\right)^2$$
$$\left.+\frac{1}{8}\left\{F_n\left(1-\frac{x}{2L}\right)^{p_x} + F_{n1}\right\}\left(\frac{d^2w_z}{dx^2}\right)^2 + \frac{1}{2}\left\{B_n\left(1-\frac{x}{2L}\right)^{p_x} + B_{n1}\right\}\left(\frac{d^2w_b}{dx^2}\right)\left(\frac{d^2w_s}{dx^2}\right)\right.$$

$$+\frac{1}{2}\left\{D_n\left(1-\frac{x}{2L}\right)^{p_x}+D_{n1}\right\}\left(\frac{d^2w_b}{dx^2}\right)\left(\frac{d^2w_z}{dx^2}\right)+\frac{1}{4}\left\{H_n\left(1-\frac{x}{2L}\right)^{p_x}+H_{n1}\right\}\left(\frac{d^2w_s}{dx^2}\right)\left(\frac{d^2w_z}{dx^2}\right)$$
$$+\frac{1}{8}\left\{X_n\left(1-\frac{x}{2L}\right)^{p_x}+X_{n1}\right\}\left(\frac{dw_s}{dx}\right)^2+\frac{1}{8}\left\{Y_n\left(1-\frac{x}{2L}\right)^{p_x}+Y_{n1}\right\}\left(\frac{dw_z}{dx}\right)^2$$
$$+\frac{1}{4}\left\{Z_n\left(1-\frac{x}{2L}\right)^{p_x}+Z_{n1}\right\}\left(\frac{dw_s}{dx}\right)\left(\frac{dw_z}{dx}\right)+2q(w_b+w_s)\Big]dx \qquad (18)$$

2.5 Finite Element Formulation

A two-node C^1 beam element with seven degrees of freedom is developed. According to the variational statement given in Eq. (18), the axial displacement u must be only once differentiable and is expressed over each element by a linear polynomial ψ_j whereas the bending, shear and thickness stretching components, w_b, w_s and w_z, must be twice differentiable and are expressed by a Hermite-cubic polynomial φ_j. The displacement functions u(x), $w_b(x)$, $w_s(x)$ and $w_z(x)$ within an element are presented as:

$$u(x)=\sum_{j=1}^{2}u_j\psi_j(x), \qquad (19a)$$

$$w_b(x)=\sum_{j=1}^{4}w_{b_j}\varphi_j(x), \qquad (19b)$$

$$w_s(x)=\sum_{j=1}^{4}w_{s_j}\varphi_j(x), \qquad (19c)$$

$$w_z(x)=\sum_{j=1}^{4}w_{z_j}\varphi_j(x), \qquad (19d)$$

Substituting Eq. (19) into Eq. (18) and then using the principle of the minimum potential energy given by Eq. (20), the system of equations to be solved for unknown variables are obtained.

$$\frac{\partial\Pi}{\partial u_j}=0,\quad \frac{\partial\Pi}{\partial w_{b_j}}=0,\quad \frac{\partial\Pi}{\partial w_{s_j}}=0,\quad \frac{\partial\Pi}{\partial w_{z_j}}=0 \qquad (20)$$

The system of equations can be expressed as the finite element model of a typical element:

$$[K]\{\Delta\}=\{F\} \qquad (21a)$$

$$\begin{bmatrix}[K_{11}] & [K_{12}] & [K_{13}] & [K_{14}]\\ [K_{12}]^T & [K_{22}] & [K_{23}] & [K_{24}]\\ [K_{13}]^T & [K_{23}]^T & [K_{33}] & [K_{34}]\\ [K_{14}]^T & [K_{24}]^T & [K_{34}]^T & [K_{44}]\end{bmatrix}\begin{Bmatrix}\{U\}\\ \{W_b\}\\ \{W_s\}\\ \{W_z\}\end{Bmatrix}=\begin{Bmatrix}\{0\}\\ \{F_2\}\\ \{F_3\}\\ \{F_4\}\end{Bmatrix} \qquad (21b)$$

where $\{\Delta\}$ is the nodal displacements, $[K]$ and $\{F\}$ are the element stiffness matrix and the element force vector respectively. $[K]$ and $\{F\}$ can be given by:

$$K_{11}(i,j) = \int_0^l \left[A\left(1-\frac{x}{2L}\right)^{p_x} + A_1\right]\psi_{i,x}\psi_{j,x}dx, \tag{22a}$$

$$K_{12}(i,j) = -\int_0^l \left[B\left(1-\frac{x}{2L}\right)^{p_x} + B_1\right]\psi_{i,x}\varphi_{j,xx}dx, \tag{22b}$$

$$K_{13}(i,j) = -\int_0^l \left[B_s\left(1-\frac{x}{2L}\right)^{p_x} + B_{s1}\right]\psi_{i,x}\varphi_{j,xx}dx, \tag{22c}$$

$$K_{14}(i,j) = \int_{-0}^l \left[X\left(1-\frac{x}{2L}\right)^{p_x} + X_1\right]\psi_{i,x}\varphi_j dx, \tag{22d}$$

$$K_{22}(i,j) = \int_0^l \left[D\left(1-\frac{x}{2L}\right)^{p_x} + D_1 + \frac{1}{2}\left\{A_n\left(1-\frac{x}{2L}\right)^{p_x} + A_{n1}\right\}\right]\varphi_{i,xx}\varphi_{j,xx}dx \tag{22e}$$

$$K_{23}(i,j) = \int_0^l \left[D_s\left(1-\frac{x}{2L}\right)^{p_x} + D_{s1} + \frac{1}{4}\left\{B_n\left(1-\frac{x}{2L}\right)^{p_x} + B_{n1}\right\}\right]\varphi_{i,xx}\varphi_{j,xx}dx \tag{22f}$$

$$K_{24}(i,j) = -\int_0^l \left[Y\left(1-\frac{x}{2L}\right)^{p_x} + Y_1\right]\varphi_{i,xx}\varphi_j dx + \frac{1}{4}\int_0^l \left[D_n\left(1-\frac{x}{2L}\right)^{p_x} + D_{n1}\right]\varphi_{i,xx}\varphi_{j,xx}dx \tag{22g}$$

$$K_{33}(i,j) = \int_0^l \left[H\left(1-\frac{x}{2L}\right)^{p_x} + H_1 + \frac{1}{8}\left\{C_n\left(1-\frac{x}{2L}\right)^{p_x} + C_{n1}\right\}\right]\varphi_{i,xx}\varphi_{j,xx}dx + \int_0^l \left[A_s\left(1-\frac{x}{2L}\right)^{p_x} + A_{s1} + \frac{1}{8}\left\{X_n\left(1-\frac{x}{2L}\right)^{p_x} + X_{n1}\right\}\right]\varphi_{i,x}\varphi_{j,x}dx \tag{22h}$$

$$K_{34}(i,j) = -\int_0^l \left[Y_s\left(1-\frac{x}{2L}\right)^{p_x} + Y_{s1}\right]\varphi_{i,xx}\varphi_j dx + \int_0^l \left[A_s\left(1-\frac{x}{2L}\right)^{p_x} + A_{s1} + \frac{1}{8}\left\{Z_n\left(1-\frac{x}{2L}\right)^{p_x} + Z_{n1}\right\}\right]\varphi_{i,x}\varphi_{j,x} dx + \frac{1}{8}\int_0^l \left[H_n\left(1-\frac{x}{2L}\right)^{p_x} + H_{n1}\right]\varphi_{i,xx}\varphi_{j,xx} dx \quad (22i)$$

$$K_{44}(i,j) = \int_0^l \left[Z\left(1-\frac{x}{2L}\right)^{p_x} + Z_1\right]\varphi_i\varphi_j dx + \int_0^l \left[A_s\left(1-\frac{x}{2L}\right)^{p_x} + A_{s1} + \frac{1}{8}\left\{Y_n\left(1-\frac{x}{2L}\right)^{p_x} + Y_{n1}\right\}\right]\varphi_{i,x}\varphi_{j,x} dx + \frac{1}{8}\int_0^l \left[F_n\left(1-\frac{x}{2L}\right)^{p_x} + F_{n1}\right]\varphi_{i,xx}\varphi_{j,xx} dx \quad (22j)$$

$$F_2(i) = -\int_0^l q\varphi_i \, dx \quad (22k)$$

$$F_3(i) = -\int_0^l q\varphi_i \, dx \quad (22l)$$

$$F_4(i) = -\int_0^l qg\varphi_i \, dx \quad (22m)$$

It should be worth noting that the x which is given in the equations above must be modified according to the location of each element in the problem domain.

3. Numerical Results

In this section, a number of numerical examples are presented for various aspect ratios, gradient indexes and material length scale parameters to investigate the flexural behaviours of the conventional FG and 2D-FG microbeams with arbitrary boundary conditions, namely simply-supported (SS), clamped-clamped (CC) and clamped-free (CF). The kinematic boundary conditions are given in Table 1. The material length scale parameter is set to $\ell = 15\mu m$ throughout examples [36]. The height and width of the microbeam are equal to each other (b=h).

Unless otherwise stated, the material properties of the two constitutes are given as ceramic (Al_2O_3): $E_1 = 380$ GPa and $\nu_1 = 0.3$ and metal (Aluminum) $E_2 = 70$ GPa and $\nu_2 = 0.3$

For convenience, dimensionless transverse displacements of the beams are defined as:

$$\bar{w} = \frac{100E_2bh^3}{q_0L^4}W(L/2,z) \text{ for SS and CC beams} \tag{23a}$$

$$\bar{w} = \frac{100E_2bh^3}{q_0L^4}W(L,z) \text{ for CF beam} \tag{23b}$$

and their dimensionless axial, normal and shear stresses are given by:

$$\bar{\sigma}_x = \frac{bh}{q_0L}\sigma_x(x,z) \tag{24a}$$

$$\bar{\sigma}_z = \frac{bh}{q_0L}\sigma_z(x,z) \tag{24b}$$

$$\bar{\sigma}_{xz} = \frac{bh}{q_0L}\sigma_{xz}(x,z) \tag{24c}$$

3.1 Flexural analysis of FG microbeams

This section is dedicated to study the static deformations of the conventional FG microbeams. All the equations needed for this part can be obtained by setting $p_x = 0$ in Eq. (22). To validate the developed FEM code, simply supported FG microbeams under uniformly distributed load are studied. The following material properties are used: ceramic (SiC): $E_1 = 427$ GPa and $\nu_1 = 0.17$ and metal (Aluminum) $E_2 = 70$ GPa and $\nu_2 = 0.3$. The computed results are compared with those from a previous study [43], which was performed with the present quasi-3D theory and Navier solution based on the MCST. Different number of elements (6, 10, 20, 30 and 40) are employed to test the convergence of the develop code based on the mid-span deflections. Numerical results are obtained for various thickness to material length scales, gradient indexes and aspect ratios. As it is seen from Table 2, the obtained results show excellent agreement with those from the previous study. It is clear that the numerical results computed by employing 20 elements are satisfactory and thus this number of elements is used from now on to carry out the extensive analysis of the FG microbeams.

The deflections of FG microbeams for various boundary conditions are presented in Tables 3 and 4. It should be noted that results of macrobeams ($h/\ell = \infty$) are also given to compare with previous results [76] using the same theory. It can be seen that the present results agree well with previous ones for macrobeams. As expected, an increment on the aspect ratio increases the deflections. It is explicit that the deflections increase as the gradient indexes and the

thickness to material length scale increase. Due to the strong size effect, the lowest deflections are always obtained when $h/\ell = 1$. This is due to the fact that the strong size effect changes the mechanical properties of the microbeams and produces an increase on their stiffness.

The variation of the axial, normal and shear stresses of CF FG microbeams are plotted in Fig. 2 for various gradient indexes and two thickness to material length scales, $h/\ell = 1$ and $h/\ell = 8$. It should be noted that the maximum axial and normal stresses increase when the gradient index increases. The axial stress is tension on the bottom of the beam. However, the maximum axial stress which is at the top of the beam is compression. As it is expected, the zero traction boundary conditions are satisfied by using the present quasi-3D theory. Because of the strong size effect, all stresses for $h/\ell = 1$ are lower than those for $h/\ell = 8$. For $h/\ell = 1$, the maximum shear stress is obtained when $p_z = 1$, however, and for $h/\ell = 8$ it is observed when $p_z = 2$.

Figure 2 Right Here

3.2 Flexural analysis of 2D-FG microbeams

Since there is no data in the literature for the deflections of 2D FG microbeams, verification studies are carried out for simply supported 2D-FG beams under uniformly distributed load. The numerical calculations are obtained by setting p_z as 1. The results are given in Table 5 along with those obtained from previous study [66]. An excellent agreement with the previous results can be observed. The mid-span deflections of the SS and CC 2D-FG microbeams and the tip deflections of CF 2D-FG microbeams are presented in Tables 6-9. It is clear that the results decrease as the aspect ratio increases. One may easily notice that they increase for all type of end conditions while the gradient indexes increase. It is seen that the increment in the deflections with respect to variation of the gradient index in the x-direction is larger than that in the z-direction for all type of end conditions. It is found that the deflections increase as h/ℓ

increases. It is clear that the strong size effect significantly affects the transverse deflections. This indicates that with the inclusion of couple stress, rigidity of the 2D-FG microbeam is increasing. Some new results for deflections of 2D-FG microbeams in Tables 6-9 can be used as reference for future studies.

The variations of the axial, normal and shear stresses through the thickness with respect to various h/ℓ are plotted in Fig. 3 by setting L/h= 5, p_z=1 and p_x=1. It is clear that the maximum stresses increase as the thickness to material length scale increases. The size effect vanishes when $h/\ell \geq 20$. The axial and normal stresses are tensile at the surface of the microbeam. The shear stress values are zero for both surfaces of the beam.

Figure 3 Right Here

The variation of the axial, normal and shear stresses of the CC 2D-FG microbeams is plotted in Figs. 4 to 6 to show the effects of the gradient indexes in both directions and the thickness to material length scale parameters. According to these figures, as the gradient index in the z-direction increases the maximum stresses increase. On the other hand, the maximum axial and normal stress decreases while the gradient index in the *x*-direction increases. It is explicit that the effect of the gradient index in the *z*-direction on the axial and normal stresses is more than the gradient index in the *x*-direction. Due to the strong small size effect, the effect of the both gradient indexes on the axial and normal stresses is more significant for lower h/ℓ than higher one. It is found that as the gradient index in the *z*-direction increases, the maximum dimensionless shear stress decreases (Fig. 6). Besides, the variation of the gradient index in the *x*-direction has different effect on the shear stress which depends on the thickness to material length scale. It is observed that the maximum shear stress value is obtained with the gradient index in the *x*-direction as 5.

Figure 4 Right Here

Figure 5 Right Here

Figure 6 Right Here

Finally, the variation of the tip deflections of the CF 2D-FG microbeams can be seen in Fig. 7 with respect to the thickness to material length scale parameters and gradient indexes. It is clear that the dimensionless tip deflection increases as the gradient indexes increase. Moreover, it is found that the effect of the gradient index in the *z*-direction is more pronounced than the gradient index in the *x*-direction for $p_z \leq 5$. However, for higher values of the gradient indexes, the effect of p_x becomes more significant than p_z. It is worth noting that strong small size effect decreases the effect of the gradient indexes on the tip deflections of the CF 2D-FG microbeams.

Figure 7 Right Here

4. Conclusion

The modified couple stress theory is employed for the flexural behaviour analysis of both conventional FG and 2D-FG microbeams based on the Ritz method and finite element formulation. A quasi-3D theory, which includes both normal and shear deformation, is used to study the deflections, axial, normal and shear stresses. The material properties are assumed to

vary through the thickness and longitudinal axis and follow the power-law distribution. The effects of the normal, shear deformations, boundary conditions, aspect ratios, gradient indexes and thickness to material length scale parameter on deflections, axial, normal and shear stresses are investigated. Based on the extensive analysis, the main important results are given below:

- The deflections of the 1D and 2D-FG microbeams are greatly affected by the thickness to material length scale parameter. While their thickness approach the material length scale parameter, they exhibit significant size dependent behaviour. The size dependence decreases while the thickness to material length scale parameter increases.
- As the gradient indexes increase, the deflections increase for all type of boundary conditions, aspect ratios and thickness to material length scale parameters.
- The increment in the deflections because of the gradient index variation in the *x*-direction is more than the gradient index variation in the *z*-direction for all type of boundary conditions.
- The influence of the gradient index in the *z*-direction on the axial and normal stresses is more pronounced than the gradient index in the *x*-direction.
- Due to the strong small size effect, the effect of the both gradient indexes on the axial and normal stresses is more significant for lower thickness to material length scale parameter.
- To meet the design requirements, the flexural behaviour of the 2D-FG microbeams can be controlled by selecting suitable gradient indexes.

References

[1] Koizumi M. FGM activities in Japan. Composites Part B: Engineering. 1997;28B:1-4

[2] Yang F, Chong ACM, Lam DCC, Tong P. Couple stress based strain gradient theory for elasticity. International Journal of Solids and Structures. 2002;39:2731–43

[3] Toupin RA. Elastic materials with couple stresses. Archives of Rational of Mechanical and Analysis. 1962;11:385–414

[4] Mindlin RD, Tiersten HF. Effects of couple-stresses in linear elasticity. Archives of Rational Mechanics and Analysis. 1962;11:415–48

[5] Koiter WT. Couple stresses in the theory of elasticity. I and II Proc K Ned Akad Wet 1964;B(67):17-44

[6] Mindlin RD. Micro-structure in linear elasticity. Archives of Rational Mechanics and Analysis. 1964;16:51-78

[7] Park SK, Gao XL. Bernoulli–Euler beam model based on a modified couple stress theory. Journal of Micromechanics and Microengineering. 2006;16(11):2355-9

[8] Kong S, Zhou S, Nie Z, Wang K. The size-dependent natural frequency of Bernoulli–Euler microbeams. International Journal of Engineering Science. 2008;46(5):427-37

[9] Xia W, Wang L, Yin L. Nonlinear non-classical microscale beams: Static bending, postbuckling and free vibration. International Journal of Engineering Science. 2010;48(12):2044-53

[10] Ma H, Gao X, Reddy J. A microstructure-dependent Timoshenko beam model based on a modified couple stress theory. Journal of the Mechanics and Physics of Solids. 2008;56(12):3379-91

[11] Asghari M, Ahmadian MT, Kahrobaiyan MH, Rahaeifard M. On the size-dependent behavior of functionally graded micro-beams. Materials & Design. 2010;31(5):2324-9

[12] Ke L-L, Wang Y-S. Size effect on dynamic stability of functionally graded microbeams based on a modified couple stress theory. Composite Structures. 2011;93(2):342-50

[13] Ke L-L, Wang Y-S, Yang J, Kitipornchai S. Nonlinear free vibration of size-dependent functionally graded microbeams. International Journal of Engineering Science. 2012;50(1):256-67

[14] Dehrouyeh-Semnani AM, Mostafaei H, Nikkhah-Bahrami M. Free flexural vibration of geometrically imperfect functionally graded microbeams. International Journal of Engineering Science. 2016;105:56-79

[15] Reddy JN. Microstructure-dependent couple stress theories of functionally graded beams. Journal of the Mechanics and Physics of Solids. 2011;59(11):2382-99

[16] Şimşek M, Kocatürk T, Akbaş ŞD. Static bending of a functionally graded microscale Timoshenko beam based on the modified couple stress theory. Composite Structures. 2013;95:740-7

[17] Kahrobaiyan MH, Asghari M, Ahmadian MT. A Timoshenko beam element based on the modified couple stress theory. International Journal of Mechanical Sciences. 2014;79:75-83

[18] Thai H-T, Vo TP, Nguyen T-K, Lee J. Size-dependent behavior of functionally graded sandwich microbeams based on the modified couple stress theory. Composite Structures. 2015;123:337-49

[19] Nateghi A, Salamat-talab M. Thermal effect on size dependent behavior of functionally graded microbeams based on modified couple stress theory. Composite Structures. 2013;96:97-110

[20] Akgöz B, Civalek Ö. Free vibration analysis of axially functionally graded tapered Bernoulli–Euler microbeams based on the modified couple stress theory. Composite Structures. 2013;98:314-22

[21] Filippi M, Carrera E. Bending and vibrations analyses of laminated beams by using a zig-zaglayer-wise theory. Composites Part B: Engineering. 2016;98:269-80

[22] Frikha A, Hajlaoui A, Wali M, Dammak F. A new higher order C0 mixed beam element for FGM beams analysis. Composites Part B: Engineering. 2016;106:181-9

[23] Giunta G, De Pietro G, Nasser H, Belouettar S, Carrera E, Petrolo M. A thermal stress finite element analysis of beam structures by hierarchical modelling. Composites Part B: Engineering. 2016;95:179-95

[24] Gupta A, Talha M, Singh BN. Vibration characteristics of functionally graded material plate with various boundary constraints using higher order shear deformation theory. Composites Part B: Engineering. 2016;94:64-74

[25] Li D, Deng Z, Xiao H. Thermomechanical bending analysis of functionally graded sandwich plates using four-variable refined plate theory. Composites Part B: Engineering. 2016;106:107-19

[26] Mantari JL, Canales FG. Finite element formulation of laminated beams with capability to model the thickness expansion. Composites Part B: Engineering. 2016;101:107-15

[27] Nguyen T-K, Nguyen V-H, Chau-Dinh T, Vo TP, Nguyen-Xuan H. Static and vibration analysis of isotropic and functionally graded sandwich plates using an edge-based MITC3 finite elements. Composites Part B: Engineering. 2016;107:162-73

[28] Hui Y, Giunta G, Belouettar S, Huang Q, Hu H, Carrera E. A free vibration analysis of threedimensional sandwich beams using hierarchical one-dimensional finite elements. Composites Part B: Engineering. 2017;110:7-19

[29] Mechab I, El Meiche N, Bernard F. Analytical study for the development of a new warping function for high order beam theory. Composites Part B: Engineering. 2017;119:18-31

[30] Shao D, Hu S, Wang Q, Pang F. Free vibration of refined higher-order shear deformation composite laminated beams with general boundary conditions. Composites Part B: Engineering. 2017;108:75-90

[31] Nateghi A, Salamat-talab M, Rezapour J, Daneshian B. Size dependent buckling analysis of functionally graded micro beams based on modified couple stress theory. Applied Mathematical Modelling. 2012;36(10):4971-87

[32] Salamat-talab M, Nateghi A, Torabi J. Static and dynamic analysis of third-order shear deformation FG micro beam based on modified couple stress theory. International Journal of Mechanical Sciences. 2012;57(1):63-73

[33] Ansari R, Gholami R, Faghih Shojaei M, Mohammadi V, Sahmani S. Size-dependent bending, buckling and free vibration of functionally graded Timoshenko microbeams based on the most general strain gradient theory. Composite Structures. 2013;100:385-97

[34] Sahmani S, Ansari R. Size-dependent buckling analysis of functionally graded third-order shear deformable microbeams including thermal environment effect. Applied Mathematical Modelling. 2013;37(23):9499-515

[35] Mohammad-Abadi M, Daneshmehr AR. Size dependent buckling analysis of microbeams based on modified couple stress theory with high order theories and general boundary conditions. International Journal of Engineering Science. 2014;74:1-14

[36] Şimşek M, Reddy JN. Bending and vibration of functionally graded microbeams using a new higher order beam theory and the modified couple stress theory. International Journal of Engineering Science. 2013;64:37-53

[37] Akgöz B, Civalek Ö. Thermo-mechanical buckling behavior of functionally graded microbeams embedded in elastic medium. International Journal of Engineering Science. 2014;85:90-104

[38] Akgöz B, Civalek Ö. Shear deformation beam models for functionally graded microbeams with new shear correction factors. Composite Structures. 2014;112:214-25

[39] Darijani H, Mohammadabadi H. A new deformation beam theory for static and dynamic analysis of microbeams. International Journal of Mechanical Sciences. 2014;89:31-9

[40] Al-Basyouni KS, Tounsi A, Mahmoud SR. Size dependent bending and vibration analysis of functionally graded micro beams based on modified couple stress theory and neutral surface position. Composite Structures. 2015;125:621-30

[41] Arbind A, Reddy JN. Nonlinear analysis of functionally graded microstructure-dependent beams. Composite Structures. 2013;98:272-81

[42] Arbind A, Reddy JN, Srinivasa AR. Modified Couple Stress-Based Third-Order Theory for Nonlinear Analysis of Functionally Graded Beams. Latin American journal of solids and structures. 2014;11:459-87

[43] Trinh LC, Nguyen HX, Vo TP, Nguyen T-K. Size-dependent behaviour of functionally graded microbeams using various shear deformation theories based on the modified couple stress theory. Composite Structures. 2016;154:556-72

[44] Apuzzo A, Barretta R, Canadija M, Feo L, Luciano R, Marotti de Sciarra F. A closed-form model for torsion of nanobeams with an enhanced nonlocal formulation. Composites Part B: Engineering. 2017;108:315-24

[45] Romano G, Barretta R. Stress-driven versus strain-driven nonlocal integral model for elastic nanobeams. Composites Part B: Engineering. 2017;114:184-8

[46] Barretta R, Feo L, Luciano R, Marotti de Sciarra F. Application of an enhanced version of the Eringen differential model to nanotechnology. Composites Part B: Engineering. 2016;96:274-80

[47] Barretta R, Feo L, Luciano R, Marotti de Sciarra F, Penna R. Functionally graded Timoshenko nanobeams: A novel nonlocal gradient formulation. Composites Part B: Engineering. 2016;100:208-19

[48] Barretta R, Feo L, Luciano R, Marotti de Sciarra F. An Eringen-like model for Timoshenko nanobeams. Composite Structures. 2016;139:104-10

[49] Barretta R, Čanadija M, Feo L, Luciano R, Marotti de Sciarra F, Penna R. Exact solutions of inflected functionally graded nano-beams in integral elasticity. Composites Part B. In Press (2017). Doi: 10.1016/j.compositesb.2017.12.022

[50] Romano G, Barretta R, Diaco M. On nonlocal integral models for elastic nano-beams. International Journal of Mechanical Sciences. 2017;131-132:490-499

[51] Romano G, Barretta R. Nonlocal elasticity in nanobeams: the stress-driven integral model. International Journal of Engineering Science. 2017;115:14-27

[52] Mindlin RD. Second gradient of strain and surface tension in linear elasticity. Archive for Rational Mechanics and Analysis. 1965;16:51-78

[53] Fleck NA, Hutchinson JW. A reformulation of strain gradient plasticity. Journal of the Mechanics and Physics of Solids. 2001;49:2245-71

[54] Lam DCC, Yang F, Chong ACM, Wang J, Tong P. Experiments and theory in strain gradient elasticity. Journal of the Mechanics and Physics of Solids. 2003;51(8):1477-508

[55] Romano G, Barretta R, Diaco M. Micromorphic continua: non-redundant formulations. Continuum Mechanics and Thermodynamics. 2016;28(6):1659-70

[56] Thai H-T, Vo TP, Nguyen T-K, Kim S-E. A review of continuum mechanics models for size-dependent analysis of beams and plates. Composite Structures. 2017;177:196-219

[57] Nemat-Alla M. Reduction of thermal stresses by developing two-dimensional functionally graded materials. International Journal of Solids and Structures. 2003;40:7339–7356.

[58] Goupee AJ, Vel SS. Optimization of natural frequencies of bidirectional functionally graded beams. Structural and Multidisciplinary Optimization. 2006;32:473–484.

[59] Lü CF, Chen WQ, Xu RQ, Lim CW. Semi-analytical elasticity solutions for bidirectional functionally graded beams. International Journal of Solids and Structures. 2008;45:258–275.

[60] Zhao L, Chen WQ, Lü CF. Symplectic elasticity for two-directional functionally graded materials. Mechanics of Materials. 2012;54:32–42.

[61] Simsek M. Bi-directional functionally graded materials (BDFGMs) for free and forced vibration of Timoshenko beams with various boundary conditions. Composite Structures. 2015;133:968-978.

[62] Simsek M. Buckling of Timoshenko beams composed of two-dimensional functionally graded material (2D-FGM) having different boundary conditions. Composite Structures. 2016;149:304–314.

[63] Karamanli A. Elastostatic analysis of two-directional functionally graded beams using various beam theories and Symmetric Smoothed Particle Hydrodynamics method. Composite Structures. 2017;160:653-669.

[64] Nazargah M. Fully coupled thermo-mechanical analysis of bi-directional FGM beams using NURBS isogeometric finite element approach. Aerospace Science and Technology. 2015;45:154-164.

[65] Pydah A, Batra RC. Shear deformation theory using logarithmic function for thick circular beams and analytical solution for bi-directional functionally graded circular beams. Composite Structures. 2017;172:45-60.

[66] Karamanli A. Bending behaviour of two directional functionally graded sandwich beams by using a quasi-3d shear deformation theory. Composite Structures. 2017;174:70-86.

[67] Barretta R. On Cesàro-Volterra method in orthotropic Saint-Venant beam. Journal of Elasticity. 2013;112(2):233-253

[68] Barretta R. On the relative position of twist and shear centres in the orthotropic and fiberwise homogeneous Saint-Venant beam theory. International Journal of Solids and Structures. 2012;49(21):3038-3046

[69] Barretta R. Analogies between Kirchhoff plates and Saint-Venant beams under torsion. Acta Mechanica. 2013;224(12):2955-2964.

[70] Nejad MZ, Hadi A. Eringen's non-local elasticity theory for bending analysis of bi-directional functionally graded Euler–Bernoulli nano-beams. International Journal of Engineering Science. 2016;106:1-9.

[71] Nejad MZ, Hadi A. Non-local analysis of free vibration of bi-directional functionally graded Euler–Bernoulli nano-beams. International Journal of Engineering Science. 2016;105:1-11.

[72] Nejad MZ, Hadi A, Rastgoo A. Buckling analysis of arbitrary two-directional functionally graded Euler–Bernoulli nano-beams based on nonlocal elasticity theory. International Journal of Engineering Science. 2016;103:1-10

[73] Shafiei N, Kazemi M. Buckling analysis on the bi-dimensional functionally graded porous tapered nano-/micro-scale beams. Aerospace Science and Technology. 2017;66:1-11

[74] Shafiei N, Mirjavadi SS, Mohasel Afshari B, Rabby S, Kazemi M. Vibration of two-dimensional imperfect functionally graded (2D-FG) porous nano-/micro-beams. Computer Methods in Applied Mechanics and Engineering. 2017;322:615-32

[75] Trinh LC, Vo TP, Thai HT, Nguyen TK. Size-dependent vibration of bi-directional functionally graded microbeams with arbitrary boundary conditions. Composites Part B: Engineering. 2017, In Press.

[76] Vo TP, Thai HT, Nguyen TK, Inam F and Lee J. Static behaviour of functionally graded sandwich beams using a quasi-3D theory. Composites Part B: Engineering. 2015; 68:591-774.

Table Captions

Table 1: Kinematic boundary conditions used for the numerical computations.

Table 2: Dimensionless mid-span deflections of SS FG microbeams for various gradient indexes.

Table 3: Dimensionless mid-span deflections of CC FG microbeams for various gradient indexes.

Table 4: Dimensionless tip deflections of CF FG microbeams for various gradient indexes.

Table 5: Dimensionless mid-span deflections, axial and shear stress of SS 2D-FG beams–($p_z = 1$)

Table 6: Dimensionless mid-span deflections, axial and shear stress of SS 2D-FG mirobeams ($p_z = 1$)

Table 7: Dimensionless mid-span deflections of the SS 2D-FG microbeams for various gradient indexes.

Table 8: Dimensionless mid-span deflections of the CC 2D-FG microbeams for various gradient indexes.

Table 9: Dimensionless tip deflections of the CF 2D-FG microbeams for various gradient indexes.

Figure Captions

Fig. 1: Geometry and coordinate of a 2D-FG beam.

Fig. 2: Variation of dimensionless axial $\bar{\sigma}_x(L/2,z)$, normal $\bar{\sigma}_z(L/2,z)$ and shear $\bar{\sigma}_{xz}(L/2,z)$stresses for CF FG microbeams with respect to gradient indexes (L/h=5, a) $^{h}/_{\ell} = 1$, b) $^{h}/_{\ell} = 8$).

Fig. 3: Variation of dimensionless axial, normal and shear stresses for SS 2D-FG microbeams with respect to thickness to material length scale parameters (L/h=5, $p_z = p_x = 1$).

Fig. 4: Variation of dimensionless axial stress $\bar{\sigma}_x(L/2,z)$ for CC 2D-FG microbeams with respect to gradient indexes (L/h=5).

Fig. 5: Variation of dimensionless normal stress $\bar{\sigma}_z(L/2,z)$ for CC 2D- FG microbeams with respect to gradient indexes (L/h=5).

Fig. 6: Variation of dimensionless shear stress $\bar{\sigma}_{xz}(L/2,z)$ for CC 2D- FG microbeams with respect to gradient indexes (L/h=5).

Fig. 7: Variation of tip deflections for CF 2D-FG microbeams with respect to gradient indexes and thickness to material length scale parameters (L/h=5).

Table 1. Kinematic boundary conditions used for the numerical computations.

BC	x=0	x=L
SS	$u = 0, w_b = 0, w_s = 0, w_z = 0$	$w_b = 0, w_s = 0, w_z = 0$
CC	$u = 0, w_b = 0, w_s = 0, w_z = 0,$ $w_b' = 0, w_s' = 0, w_z' = 0$	$u = 0, w_b = 0, w_s = 0, w_z = 0,$ $w_b' = 0, w_s' = 0, w_z' = 0$
CF	$u = 0, w_b = 0, w_s = 0, w_z = 0,$ $w_b' = 0, w_s' = 0$	

Table 2 Dimensionless mid-span deflections of SS FG microbeams for various gradient indexes.

L/h	h/ℓ	Number of elements	Theory	$p_z = 0$	$p_z = 0.5$	$p_z = 1$	$p_z = 10$
5	1	6 elements	Present Quasi-3D	0.0364	0.0527	0.0663	0.1564
		10 elements		0.0364	0.0527	0.0663	0.1565
		20 elements		0.0364	0.0527	0.0663	0.1565
		30 elements		0.0364	0.0527	0.0663	0.1565
		40 elements		0.0364	0.0527	0.0663	0.1565
		Quasi-3D [43]		0.0364	0.0527	0.0663	0.1565
	2	6 elements	Present Quasi-3D	0.0990	0.1460	0.1859	0.4015
		10 elements		0.0990	0.1461	0.1860	0.4019
		20 elements		0.0990	0.1461	0.1861	0.4020
		30 elements		0.0990	0.1461	0.1861	0.4020
		40 elements		0.0990	0.1461	0.1861	0.4020
		Quasi-3D [43]		0.0990	0.1461	0.1861	0.4021
	4	6 elements	Present Quasi-3D	0.1734	0.2621	0.3383	0.6655
		10 elements		0.1734	0.2622	0.3388	0.6665
		20 elements		0.1734	0.2623	0.3391	0.6669
		30 elements		0.1734	0.2623	0.3391	0.6669
		40 elements		0.1734	0.2623	0.3391	0.6669
		Quasi-3D [43]		0.1734	0.2623	0.3391	0.6670
	8	6 elements	Present Quasi-3D	0.2136	0.3270	0.4256	0.7989
		10 elements		0.2136	0.3273	0.4265	0.8002
		20 elements		0.2136	0.3274	0.4268	0.8008
		30 elements		0.2136	0.3274	0.4269	0.8009
		40 elements		0.2136	0.3274	0.4269	0.8009
		Quasi-3D [43]		0.2136	0.3274	0.4269	0.8010
10	1	6 elements	Present Quasi-3D	0.0352	0.0510	0.0643	0.1520
		10 elements		0.0352	0.0510	0.0643	0.1521
		20 elements		0.0352	0.0510	0.0643	0.1521
		30 elements		0.0352	0.0510	0.0643	0.1521
		40 elements		0.0352	0.0510	0.0643	0.1521
		Quasi-3D [43]		0.0352	0.0510	0.0643	0.1521
	2	6 elements	Present Quasi-3D	0.0949	0.1404	0.1789	0.3827
		10 elements		0.0949	0.1404	0.1791	0.3831
		20 elements		0.0949	0.1404	0.1792	0.3833
		30 elements		0.0949	0.1404	0.1792	0.3833
		40 elements		0.0949	0.1404	0.1792	0.3833
		Quasi-3D [43]		0.0949	0.1404	0.1792	0.3833
	4	6 elements	Present Quasi-3D	0.1646	0.2499	0.3230	0.6181
		10 elements		0.1646	0.2501	0.3236	0.6191
		20 elements		0.1646	0.2501	0.3238	0.6195
		30 elements		0.1646	0.2502	0.3239	0.6195
		40 elements		0.1646	0.2502	0.3239	0.6195
		Quasi-3D [43]		0.1646	0.2502	0.3239	0.6196
	8	6 elements	Present Quasi-3D	0.2016	0.3105	0.4045	0.7311
		10 elements		0.2016	0.3107	0.4053	0.7324
		20 elements		0.2016	0.3108	0.4057	0.7330
		30 elements		0.2016	0.3108	0.4058	0.7331
		40 elements		0.2016	0.3108	0.4058	0.7331
		Quasi-3D [43]		0.2016	0.3109	0.4058	0.7332

Table 3 Dimensionless mid-span deflections of CC FG microbeams for various gradient indexes.

L/h	h/ℓ	Reference	$p_z = 0$	$p_z = 1$	$p_z = 2$	$p_z = 5$	$p_z = 10$
5	1	Present	0.1202	0.2068	0.2624	0.3555	0.4313
	2		0.3287	0.5831	0.7454	0.9894	1.1749
	4		0.5836	1.0747	1.3898	1.8261	2.1277
	8		0.7281	1.3680	1.7828	1.8261	2.1277
	∞		0.8217	1.5534	2.0296	2.6774	3.0951
	∞	FEM [76]	0.8327	1.5722	2.0489	2.6929	3.1058
10	1	Present	0.1060	0.1839	0.2367	0.3245	0.3927
	2		0.2755	0.4989	0.6419	0.8427	0.9883
	4		0.4599	0.8733	1.1248	1.4174	1.6143
	8		0.5530	1.0760	1.3873	1.7168	1.9294
	∞		0.6306	1.2303	1.5810	1.9471	2.1905
20	1	Present	0.1021	0.1776	0.2297	0.3159	0.3820
	2		0.2607	0.4755	0.6131	0.8014	0.9356
	4		0.4265	0.8190	1.0529	1.3054	1.4734
	8		0.5072	0.9996	1.2833	1.5509	1.7237
	∞		0.5845	1.1522	1.4704	1.7623	1.9593
	∞	FEM [76]	0.5894	1.1613	1.4811	1.7731	1.9694

Table 4 Dimensionless tip deflections of CF FG microbeams for various gradient indexes.

L/h	h/ℓ	Reference	$p_z = 0$	$p_z = 1$	$p_z = 2$	$p_z = 5$	$p_z = 10$
5	1	Present	4.9207	8.5591	11.0626	15.2093	18.3904
	2		12.5871	13.8139	15.1851	19.9476	28.0594
	4		20.6392	39.6255	50.9772	63.3044	71.4820
	8		24.5841	48.4402	62.2580	75.4226	83.8715
	∞		28.1129	55.4977	71.0212	85.5438	95.3550
	∞	FEM [76]	28.5524	56.2002	71.7295	86.1201	95.7582
10	1	Present	4.8576	8.4580	10.9493	15.0716	18.2182
	2		12.3493	22.5778	29.1321	38.0364	44.3417
	4		20.1027	38.7537	49.8245	61.5077	69.2222
	8		23.8480	47.2127	60.5900	72.7624	80.5743
	∞		27.5448	54.5183	69.5326	82.8371	91.8567
20	1	Present	4.8411	8.4317	10.9197	15.0356	18.1732
	2		12.2871	22.4799	29.0112	37.8630	44.1226
	4		19.9645	38.5294	49.2579	61.0485	68.6661
	8		23.6640	49.9070	60.1767	72.1243	79.8687
	∞		27.4872	54.4071	69.2900	82.2525	91.0326
	∞	FEM [76]	27.6217	54.6285	69.5266	82.4836	91.2606

Table 5 Dimensionless mid-span deflections, axial and shear stress of SS 2D-FG beams for various gradient indexes ($p_z = 1$)

L/h	Reference	$p_x = 0$	$p_x = 1$	$p_x = 2$	$p_x = 5$	$p_x = 10$
5	Deflections					
	Present	6.1318	7.2314	8.3533	11.3840	14.3867
	Meshless [66]	6.1343	7.2342	8.3430	-	-
	Axial stress $\bar{\sigma}_x(\frac{L}{2},\frac{h}{2})$					
	Present	5.8946	5.6360	5.3826	4.7306	4.1064
	Meshless [66]	5.8815	5.6196	5.3454	-	-
	Shear stress $\bar{\sigma}_{xz}(0,0)$					
	Present	0.7333	0.7886	0.8299	0.8787	0.8735
	Meshless [66]	0.7234	0.7780	0.8186	-	-
20	Deflections					
	Present	5.7184	6.7284	7.7680	10.6228	13.4716
	Meshless [66]	5.7215	6.7299	7.7469	-	-
	Axial stress $\bar{\sigma}_x(\frac{L}{2},\frac{h}{2})$					
	Present	23.2583	22.2396	21.2480	18.6978	16.2384
	Meshless [66]	23.2099	22.1731	21.0861	-	-
	Shear stress $\bar{\sigma}_{xz}(0,0)$					
	Present	0.7479	0.8008	0.8394	0.8798	0.8614
	Meshless [66]	0.7432	0.7993	0.8415	-	-

Table 6: Dimensionless mid-span deflections, axial and shear stress of SS 2D-FG microbeams for various gradient indexes ($p_z = 1$)

L/h	h/ℓ	Results	$p_x = 0$	$p_x = 1$	$p_x = 2$	$p_x = 5$	$p_x = 10$
5	1	Deflections	0.9136	1.1038	1.3051	1.8658	2.4156
		Axial stress $\bar{\sigma}_x(\frac{L}{2},\frac{h}{2})$	0.9527	0.9357	0.9173	0.8537	0.7618
		Shear stress $\bar{\sigma}_{xz}(0,0)$	0.1019	0.1109	0.1181	0.1289	0.1334
	8	Deflections	5.3006	6.2531	7.2242	9.8416	12.4293
		Axial stress $\bar{\sigma}_x(\frac{L}{2},\frac{h}{2})$	5.4605	5.2325	5.0083	4.4237	3.8492
		Shear stress $\bar{\sigma}_{xz}(0,0)$	0.6627	0.7158	0.7562	0.8089	0.8154
20	1	Deflections	0.8796	1.0620	1.2558	1.7996	2.3348
		Axial stress $\bar{\sigma}_x(\frac{L}{2},\frac{h}{2})$	3.8772	3.8083	3.7323	3.4746	3.1061
		Shear stress $\bar{\sigma}_{xz}(0,0)$	0.1037	0.1117	0.1178	0.1249	0.1236
	8	Deflections	4.9015	5.7663	6.6552	9.0946	11.5693
		Axial stress $\bar{\sigma}_x(\frac{L}{2},\frac{h}{2})$	21.5721	20.6743	19.7950	17.4989	15.2269
		Shear stress $\bar{\sigma}_{xz}(0,0)$	0.6735	0.7229	0.7591	0.7985	0.7846

Table 7 Dimensionless mid-span deflections of the SS 2D-FG microbeams for various gradient indexes.

h/ℓ	p_z	p_x				
		0	1	2	5	10
L/h=5						
1	0	0.5264	0.6667	0.8324	1.4065	2.1451
	1	0.9136	1.1038	1.3051	1.8658	2.4156
	2	1.1770	1.3780	1.5777	2.0814	2.5241
	5	1.6144	1.8028	1.9749	2.3580	2.6521
	10	1.9535	2.1133	2.2506	2.5306	2.7268
2	0	1.3635	1.7270	2.1552	3.6323	5.5279
	1	2.4730	2.9622	3.4727	4.8757	6.2526
	2	3.1840	3.6773	4.1636	5.3980	6.5155
	5	4.1777	4.6237	5.0413	6.0176	6.8168
	10	4.8950	5.2969	5.6555	6.4303	7.0076
4	0	2.2652	2.8691	3.5787	6.0146	9.1338
	1	4.3140	5.1162	5.9404	8.1755	10.3777
	2	5.5572	6.3187	7.0652	8.9850	10.7886
	5	6.9836	7.6478	8.2881	9.8698	11.2511
	10	7.9377	8.5703	9.1580	10.5031	11.5658
8	0	2.7142	3.4380	4.2873	7.1957	10.9163
	1	5.3006	6.2531	7.2242	9.8416	12.4293
	2	6.8322	7.7048	8.5594	10.7789	12.9084
	5	8.4154	9.1625	9.8959	11.7625	13.4458
	10	9.4327	10.1633	10.8573	12.4935	13.8246
∞	0	3.1394	3.9764	4.9588	8.3261	12.6406
	1	6.1318	7.2314	8.3533	11.3840	14.3867
	2	7.8571	8.8609	9.8488	12.4325	14.9233
	5	9.6003	10.4696	11.3292	13.5332	15.5285
	10	10.7555	11.6141	12.4344	14.3792	15.9632
L/h=20						
1	0	0.5051	0.6397	0.7994	1.3580	2.0798
	1	0.8796	1.0620	1.2558	1.7996	2.3348
	2	1.1389	1.3312	1.5229	2.0089	2.4376
	5	1.5680	1.7467	1.9102	2.2762	2.5583
	10	1.8953	2.0456	2.1750	2.4406	2.6279
2	0	1.2831	1.6248	2.0305	3.4487	5.2815
	1	2.3465	2.8061	3.2879	4.6259	5.9480
	2	3.0278	3.4868	3.9417	5.1111	6.1816
	5	3.9526	4.3624	4.7506	5.6753	6.4466
	10	4.6075	4.9796	5.3162	6.0564	6.6296
4	0	2.0868	2.6425	3.3022	5.6077	8.5899
	1	4.0245	4.7609	5.5226	7.6188	9.7091
	2	5.1734	5.8598	6.5401	8.3284	10.0477
	5	6.3824	6.9785	7.5671	9.0651	10.4389
	10	7.1842	7.7740	8.3324	9.6439	10.8226
8	0	2.4747	3.1338	3.9162	6.6508	10.2041
	1	4.9015	5.7663	6.6552	9.0946	11.5693
	2	6.2891	7.0640	7.8344	9.8933	11.9717
	5	7.5488	8.2185	8.8958	10.6865	12.5156
	10	8.3754	9.0727	9.7492	11.4176	13.1510
∞	0	2.8947	3.6656	4.5806	7.7778	11.9083
	1	5.7184	6.7284	7.7680	10.6228	13.4716
	2	7.2773	8.1819	9.0864	11.5114	13.8817
	5	8.6446	9.4404	10.2475	12.3673	14.3076
	10	9.5726	10.4004	11.1993	13.1082	14.6676

Table 8 Dimensionless mid-span deflections of the CC 2D-FG microbeams for various gradient indexes.

h/ℓ	p_z	p_x				
		0	1	2	5	10
L/h=5						
1	0	0.1202	0.1530	0.1881	0.2834	0.3751
	1	0.2068	0.2511	0.2933	0.3879	0.4623
	2	0.2624	0.3093	0.3514	0.4381	0.5008
	5	0.3555	0.4005	0.4375	0.5059	0.5505
	10	0.4313	0.4703	0.5004	0.5518	0.5831
2	0	0.3287	0.4182	0.5140	0.7739	1.0270
	1	0.5831	0.7035	0.8175	1.0728	1.2752
	2	0.7454	0.8696	0.9808	1.2120	1.3811
	5	0.9894	1.1056	1.2029	1.3868	1.5082
	10	1.1749	1.2780	1.3594	1.5019	1.5895
4	0	0.5836	0.7424	0.9119	1.3712	1.8235
	1	1.0747	1.2863	1.4852	1.9298	2.2862
	2	1.3898	1.6003	1.7889	2.1853	2.4786
	5	1.8261	2.0142	2.1746	2.4852	2.6923
	10	2.1277	2.2932	2.4277	2.6706	2.8216
8	0	0.7281	0.9261	1.1371	1.7072	2.2710
	1	1.3680	1.6302	1.8755	2.4231	2.8642
	2	1.7828	2.0378	2.2665	2.7500	3.1098
	5	2.3436	2.5624	2.7516	3.1238	3.3732
	10	2.7076	2.8960	3.0532	3.3434	3.5248
∞	0	0.8217	1.0455	1.2842	1.9315	2.5789
	1	1.5534	1.8498	2.1275	2.7528	3.2609
	2	2.0296	2.3165	2.5754	3.1292	3.5436
	5	2.6774	2.9215	3.1352	3.5616	3.8479
	10	3.0951	3.3043	3.4821	3.8145	4.0227
L/h=20						
1	0	0.1021	0.1300	0.1600	0.2412	0.3174
	1	0.1776	0.2153	0.2511	0.3312	0.3927
	2	0.2297	0.2693	0.3046	0.3771	0.4282
	5	0.3159	0.3527	0.3828	0.4382	0.4732
	10	0.3820	0.4129	0.4367	0.4770	0.5009
2	0	0.2607	0.3319	0.4084	0.6159	0.8106
	1	0.4755	0.5709	0.6609	0.8614	1.0152
	2	0.6131	0.7086	0.7942	0.9734	1.1013
	5	0.8014	0.8874	0.9611	1.1041	1.1978
	10	0.9356	1.0133	1.0764	1.1897	1.2590
4	0	0.4265	0.5430	0.6680	1.0072	1.3258
	1	0.8190	0.9728	1.1167	1.4371	1.6827
	2	1.0529	1.1977	1.3290	1.6113	1.8160
	5	1.3054	1.4328	1.5479	1.7839	1.9430
	10	1.4734	1.5973	1.7033	1.9028	2.0289
8	0	0.5072	0.6457	0.7944	1.1976	1.5767
	1	0.9996	1.1808	1.3496	1.7259	2.0145
	2	1.2833	1.4480	1.5987	1.9279	2.1688
	5	1.5509	1.6947	1.8285	2.1099	2.3027
	10	1.7237	1.8688	1.9959	2.2407	2.3989
∞	0	0.5845	0.7443	0.9160	1.3833	1.8246
	1	1.1522	1.3611	1.5563	1.9937	2.3304
	2	1.4704	1.6601	1.8350	2.2204	2.5033
	5	1.7623	1.9309	2.0886	2.4223	2.6512
	10	1.9593	2.1310	2.2818	2.5730	2.7598

Table 9 Dimensionless tip deflections of the CF 2D-FG microbeams for various gradient indexes.

h/ℓ	p_z	p_x				
		0	1	2	5	10
L/h=5						
1	0	4.9207	5.3966	5.9280	7.7744	10.9306
	1	8.5591	9.2176	9.9073	12.0027	14.9647
	2	11.0626	11.7642	12.4724	14.4905	17.1269
	5	15.2093	15.8725	16.5095	18.1870	20.1803
	10	18.3904	18.9569	19.4819	20.7907	22.2494
2	0	12.5871	13.8139	15.1851	19.9476	28.0594
	1	22.9526	24.6385	26.3913	31.6615	39.0516
	2	29.5943	31.2984	33.0100	37.8881	44.3291
	5	38.6990	40.2354	41.7351	45.8095	50.8652
	10	45.1877	46.5898	47.9222	51.3745	55.4021
4	0	20.6392	22.6665	24.9341	32.8093	46.1751
	1	39.6255	42.3839	45.2293	53.6950	65.4712
	2	50.9772	53.5889	56.2038	63.6789	73.6885
	5	63.3044	65.5574	67.7965	74.0873	82.2488
	10	71.4820	73.6709	75.7995	81.5212	88.4924
8	0	24.5841	27.0066	29.7175	39.1321	55.0853
	1	48.4402	51.7176	55.0855	65.0558	78.8740
	2	62.2580	65.2503	68.2445	76.8280	88.4163
	5	75.4226	77.9524	80.4908	87.7461	97.3660
	10	83.8715	86.3971	88.8818	95.6802	104.1344
∞	0	28.1129	30.9503	34.1270	45.1626	63.8316
	1	55.4977	59.3376	63.2867	74.9833	91.1610
	2	71.0212	74.5281	78.0478	88.1681	101.8271
	5	85.5438	88.5651	91.6046	100.3052	111.8212
	10	95.3550	98.3980	101.3950	109.5963	119.7711
L/h=20						
1	0	4.8411	5.3021	5.8161	7.6031	10.6797
	1	8.4317	9.0713	9.7407	11.7779	14.6752
	2	10.9197	11.6034	12.2928	14.2593	16.8404
	5	15.0356	15.6826	16.3033	17.9387	19.8886
	10	18.1732	18.7247	19.2355	20.5101	21.9353
2	0	12.2871	13.4576	14.7629	19.3007	27.1115
	1	22.4799	24.0957	25.7730	30.8256	37.9722
	2	29.0112	30.6453	32.2846	36.9685	43.2055
	5	37.8630	39.3348	40.7729	44.7004	49.6151
	10	44.1226	45.4711	46.7562	50.1053	54.0416
4	0	19.9645	21.8674	23.9895	31.3669	44.0623
	1	38.5294	41.1268	43.7998	51.7714	62.9997
	2	49.5279	51.9733	54.4209	61.4639	71.0389
	5	61.0485	63.1671	65.2869	71.3155	79.2469
	10	68.6661	70.7771	72.8425	78.4386	85.3157
8	0	23.6640	25.9200	28.4359	37.1824	52.2331
	1	46.9070	49.9614	53.0914	62.3851	75.4598
	2	60.1767	62.9352	65.6983	73.6990	84.7196
	5	72.1243	74.4871	76.8833	83.8431	93.2310
	10	79.8687	82.3361	84.7772	91.5034	99.9354
∞	0	27.4872	30.1290	33.0751	43.3176	60.9395
	1	54.4071	57.9786	61.6418	72.5328	87.8652
	2	69.2900	72.5125	75.7525	85.1782	98.1991
	5	82.2525	85.0696	87.9357	96.2803	107.5314
	10	91.0326	93.9935	96.9268	105.0134	115.1265

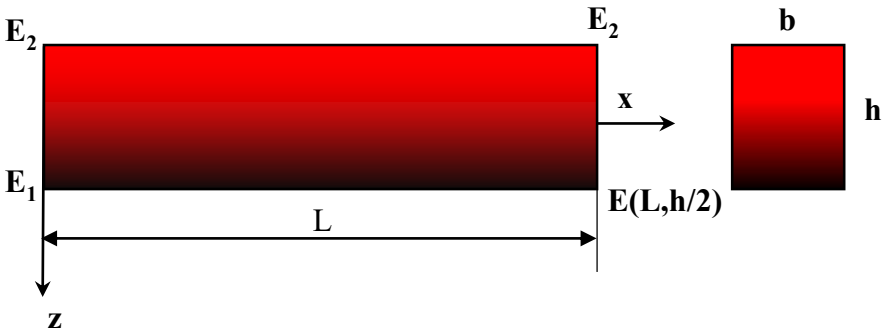

Fig. 1: Geometry and coordinate of a 2D-FG beam.

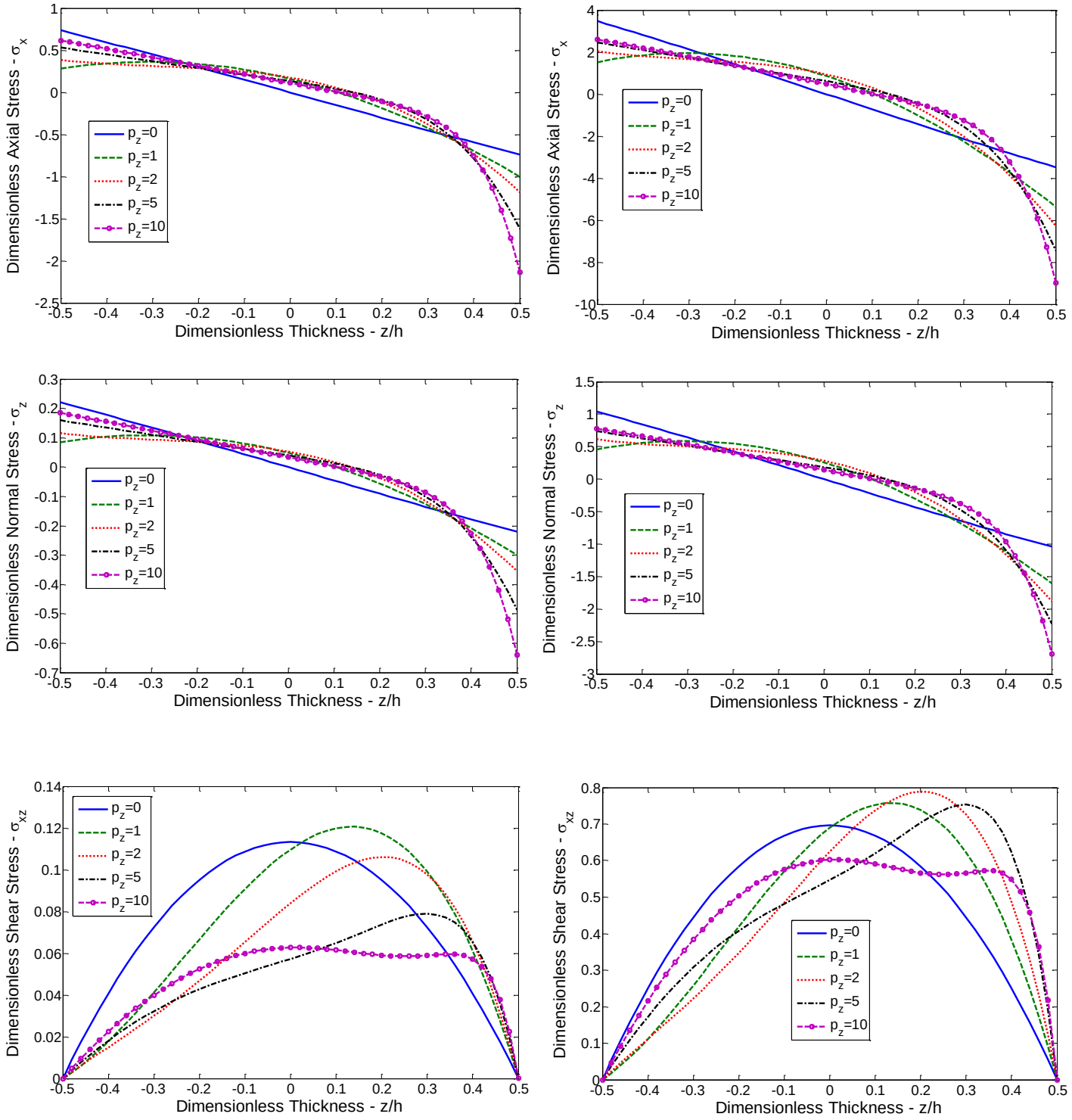

a) $h/\ell = 1$ b) $h/\ell = 8$

Fig. 2: Variation of dimensionless axial stress $\bar{\sigma}_x(L/2, z)$, normal stress $\bar{\sigma}_z(L/2, z)$ and shear stress $\bar{\sigma}_{xz}(L/2, z)$ for CF FG microbeams with respect to gradient indexes (L/h=5, $h/\ell = 1$ and $h/\ell = 8$.)

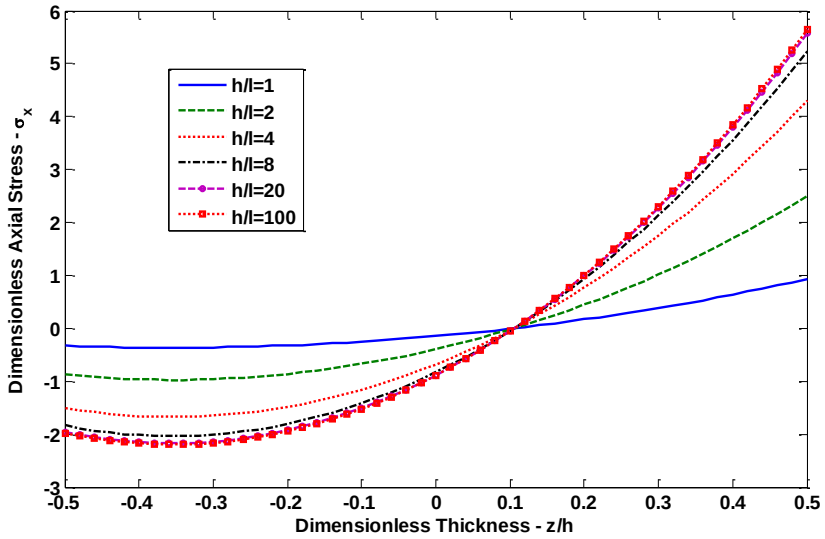

a) Axial stress $\bar{\sigma}_x(L/2,z)$

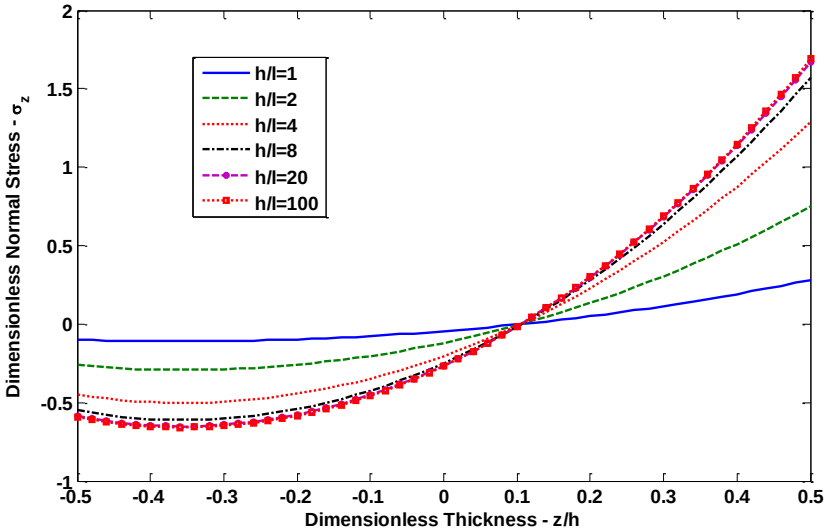

b) Normal stress $\bar{\sigma}_z(L/2,z)$

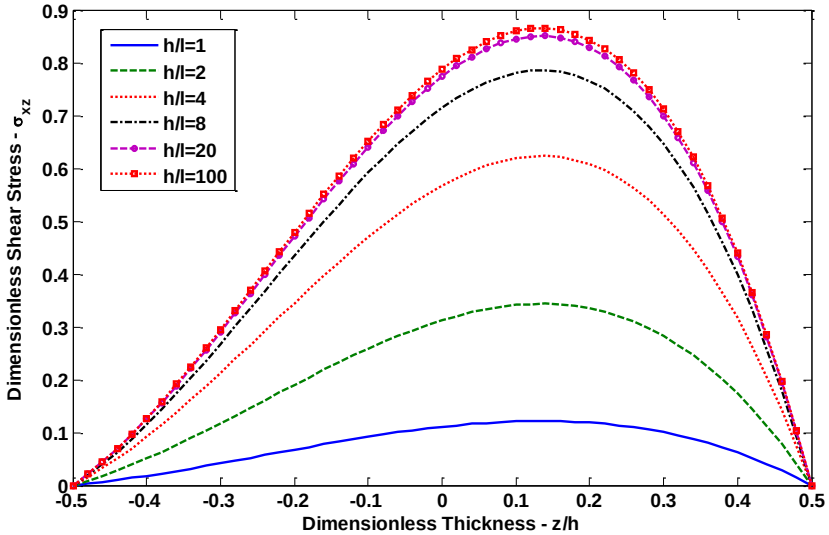

c) Shear stress $\bar{\sigma}_{xz}(0,z)$

Fig. 3: Variation of dimensionless axial, normal and shear stresses for SS 2D-FG microbeams with respect to thickness to material length scale parameters (L/h=5, $p_z = p_x = 1$).

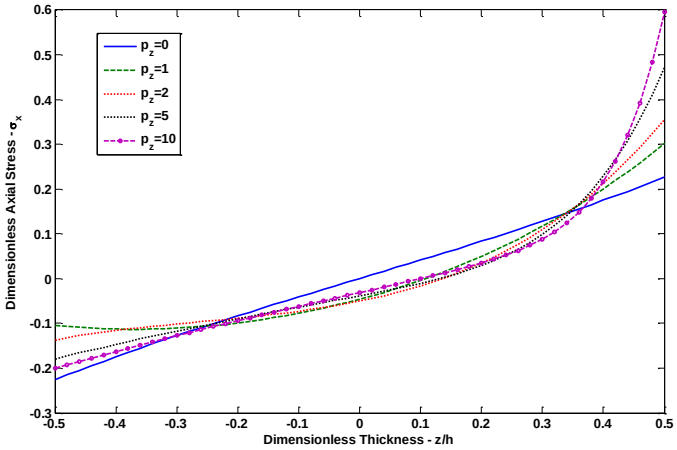

a) h/l=1, p_x=1

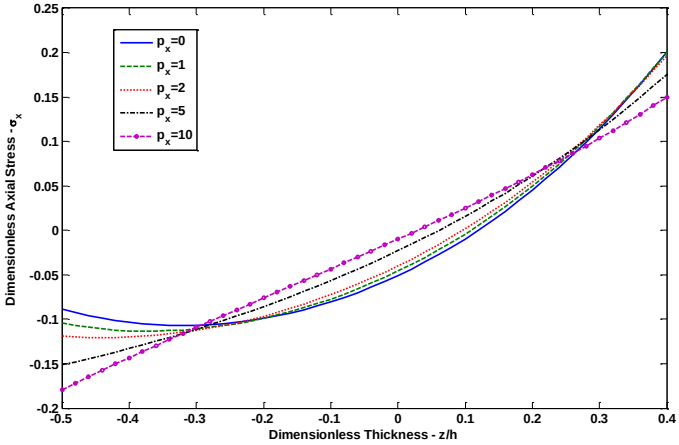

b) h/l=1, p_z=1

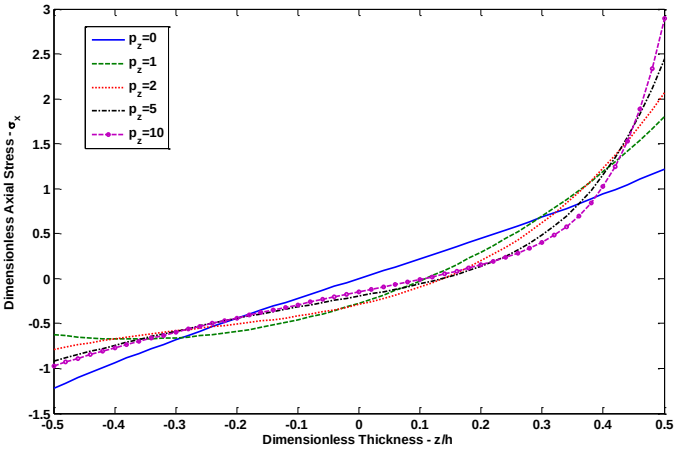

c) h/l=8, p_x=1

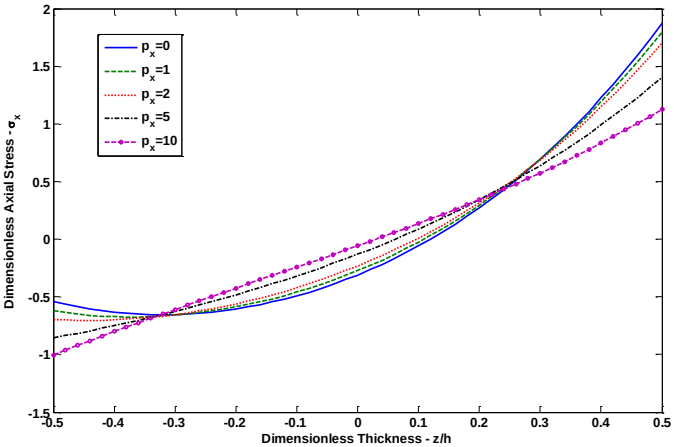

d) h/l=8, p_z=1

Fig. 4: Variation of dimensionless axial stress $\bar{\sigma}_x(L/2, z)$ for CC 2D-FG microbeams with respect to gradient indexes (L/h=5).

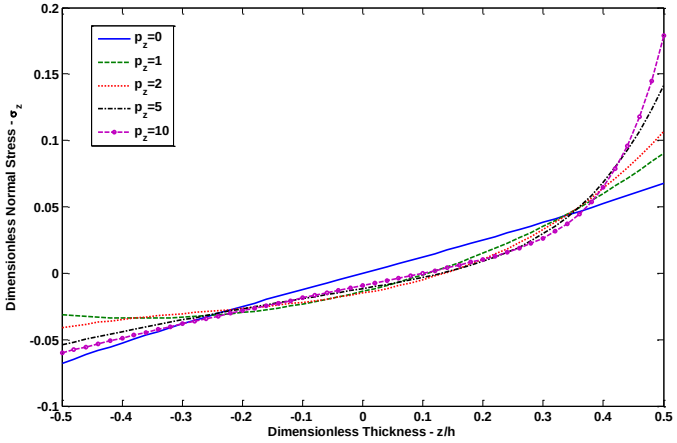

a) h/l=1, p_x=1

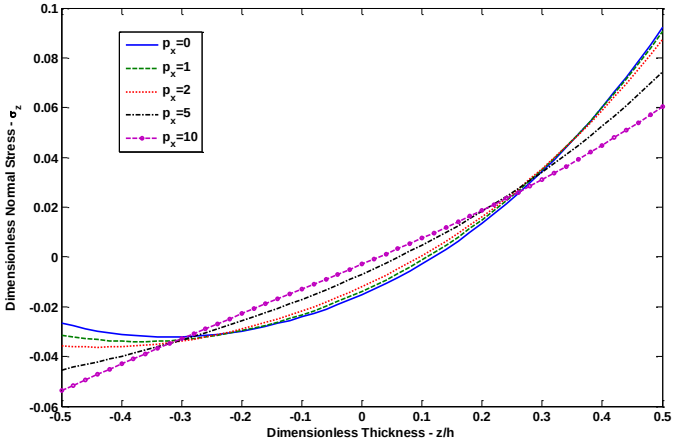

b) h/l=1, p_z=1

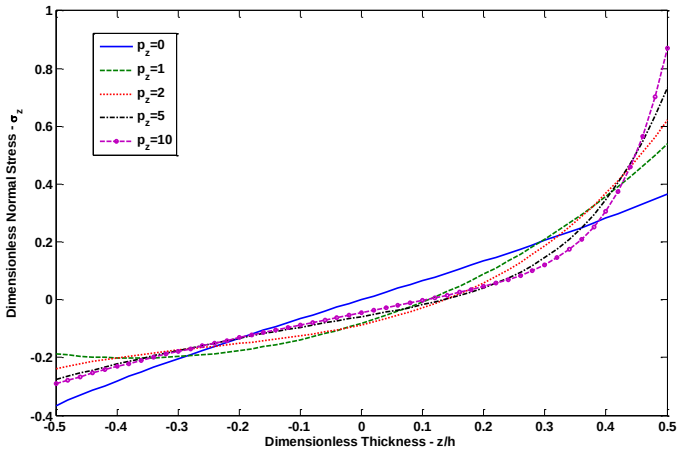

c) h/l=8, p_x=1

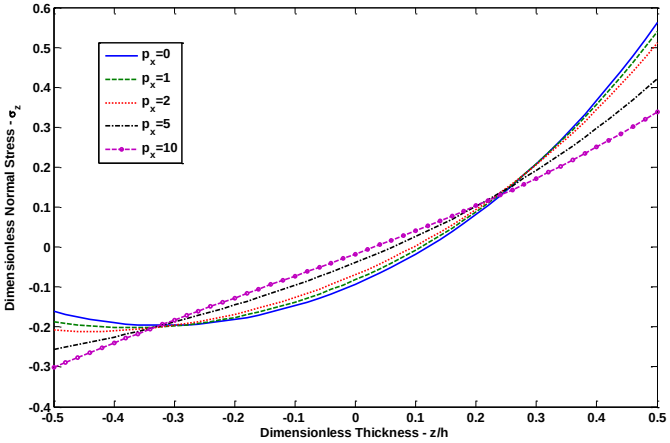

d) h/l=8, p_z=1

Fig. 5: Variation of dimensionless normal stress $\bar{\sigma}_z(L/2, z)$ for CC 2D- FG microbeams with respect to gradient indexes (L/h=5).

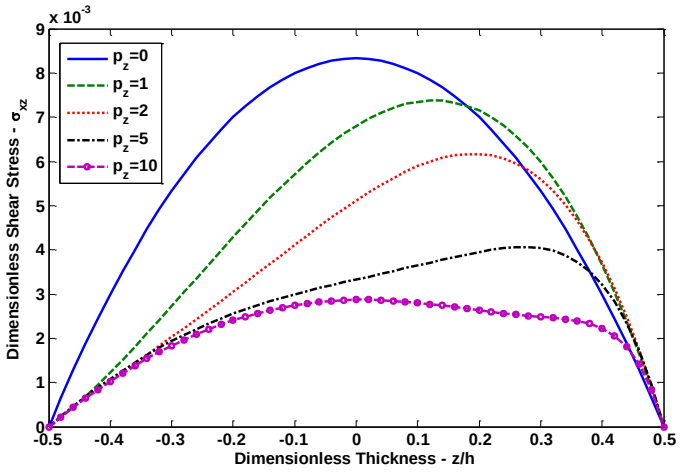

a) h/l=1, p_x=1

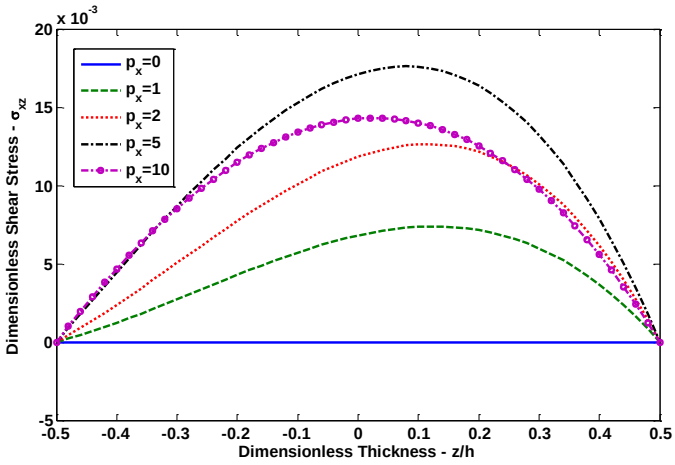

b) h/l=1, p_z=1

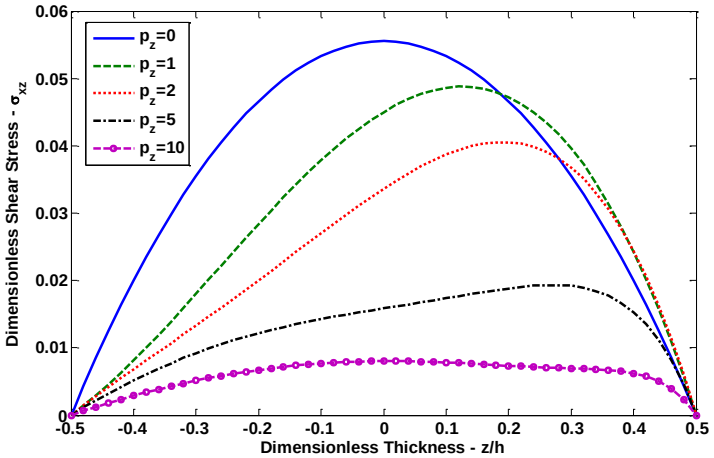

c) h/l=8, p_x=1

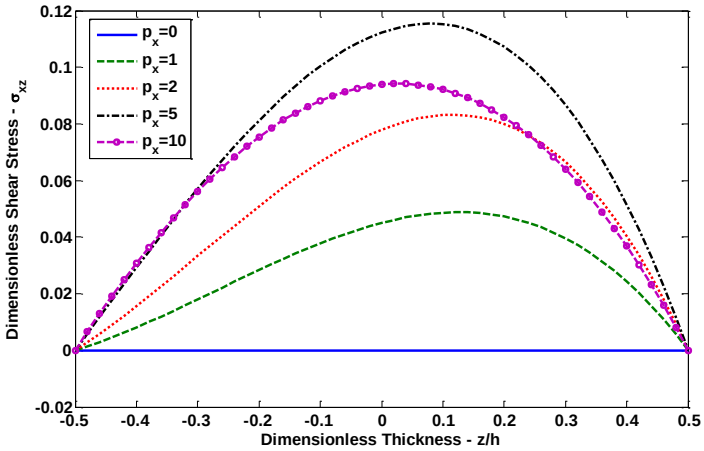

d) h/l=8, p_z=1

Fig. 6: Variation of dimensionless shear stress $\bar{\sigma}_{xz}(L/2, z)$ for CC 2D- FG microbeams with respect to gradient indexes (L/h=5).

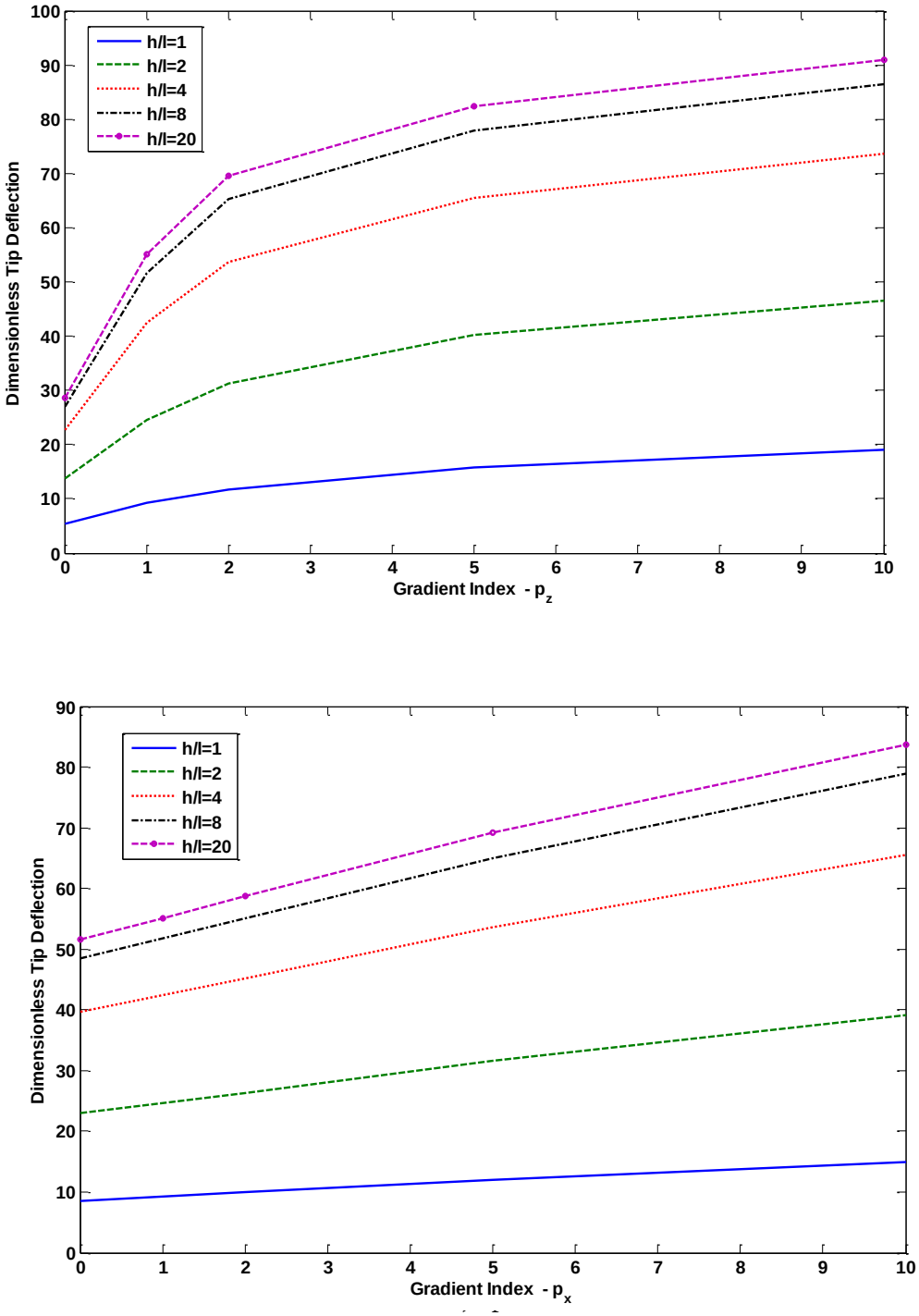

Fig. 7: Variation of tip deflections for CF 2D-FG microbeams with respect to gradient indexes and thickness to material length scale parameters (L/h=5).